Assembly of endocytic machinery around individual influenza viruses during viral entry

M. J. Rust, M. Lakadamyali, F. Zhang, X. Zhuang

Supplementary Figure

Supplementary Figure 1. Internalization of cholera toxin via caveolae. Alexa Fluor 647-conjugated cholera toxin subunit β (Molecular Probes) was incubated with cells expressing Caveolin-1-EGFP at 4°C for 15 min. After removing excess cholera toxin, the temperature was raised to 37°C to initiate endocyosis. Cholera toxin was found to localize into discrete spots (red images), all of which colocalize with caveolin-1-EGFP structures (green images). Three examples of these cholera toxin-containing structures are indicated by arrows. For each example, three consecutive images, each 10 s apart in time, are shown to illustrate the movement of these structures. Treating cells with nocodazole (60 μM) completely inhibited this movement, indicating that these EGFP-labeled caveolin structures containing cholera toxin were internalized and moving in a microtubule-dependent manner. Such structures were not observed in cells treated with filipin (5 μg/ml), an inhibitor of caveolin-dependent endocytosis, suggesting that the internalization of cholera toxin here is via caveolae. During the observation window (50–100 s), 54% of the cholera toxin-containing structures showed microtubule-dependent movement in Caveolin-1-EGFP expressing cells; and this fraction is similar in untransfected cells (52%). In both transfected and untransfected cells, we started to observe such mobile structures within 5 minutes of the initiation of endocytosis. These results indicate that the expression of Caveolin-1-EGFP did not significantly perturb caveolin-mediated endocytosis. Scale bars: 3 μm.

Supplementary Figure 2. Relative displacements of CCPs from their associated viruses. Black and red symbols are the displacements in the x and y directions in units of camera pixels (95 nm/pixel), respectively. We used least-squares fitting to determine the location of any EYFP-labeled clathrin structures near the virus prior to its stage II movement. In each frame, we considered a 4 μm^2 area centered on the virus peak. The EYFP signal in this region was fit to a Gaussian function $I(x,y) = I_0 + Ae^{-[(x-x_0)^2+(y-y_0)^2]/2\sigma^2}$, where I_0 is the average background fluorescence level, A is the amplitude of the peak, x_0 and y_0 are the center coordinates, and σ is the width. I_0, A, x_0, and y_0 were treated as free fitting parameters, while σ was fixed to be the experimentally measured width of a diffraction-limited spot. The error bars are determined from the variance matrix obtained by the least-squares fitting. Visual inspection of the movies shows that we are able track the peak as soon as a clathrin structure discernable from the background appears in the 4 μm^2 area. In 96% of the trajectories, the clathrin peak position (x_0, y_0) starts centered on the virus to within 1 pixel, as indicated by examples shown in **a-e**. Among these, only 2% of viruses seem to land on a pre-existing CCP. The rest show the appearance of a clathrin spot after viral binding. The EYFP-clathrin intensity gradually increased and then rapidly disappeared before the virus started stage II movement. After the clathrin-structure has disappeared, tracking is no longer possible, as indicated by the large error bars appearing at the end of the plots. In the remaining 4% of the trajectories, the initial clathrin peak position is separated from that of the virus (i.e. $x_0 \neq 0$ and $y_0 \neq 0$) and the separation in general decreases with time until the virus joins the clathrin structure, as shown in **f**. This quantitative analysis confirms the results of our visual inspection and indicates *de novo* formation of CCPs at the site of bound viruses.

Supplementary Figure 3. An integrated histogram of the relative time between the last CCV uncoating event prior to stage II viral movement and the onset of stage II movement. Circles indicate the number of events with the relative time shorter than value indicated on the horizontal axis. The solid curve is a fit to a double exponential decay with time constants 20 s and 270 s. These data clearly show a biphasic behaviour: while the majority of viruses started their stage II movement relatively rapidly after uncoating with a time constant of 20 s, the rest remained in the cell periphery for several minutes before stage II movement. The former population of viruses most likely stays inside the cell during the brief period between clathrin uncoating and stage II movement, as both recycling and endocytosis typical take a few minutes or longer. However, the relatively long lag between clathrin uncoating and stage II movement for the latter population leaves open the possibility that these viruses may have entered the cell via a CCP, then recycled back to the cell surface and re-entered via a clathrin-independent mechanism. We thus re-evaluate the partition ratio of viruses between the clathrin-dependent and -independent pathways by classifying endocytosis based on the internalization event immediately preceding stage II movement. This is reasonable as viral fusion was not observed without microtubule-dependent movement. In the extreme case that all of the viruses under the second phase were recycled and re-entered the cell without using a CCP, the fraction of viruses that enter via the clathrin-independent pathway would be increased from the observed 35% to 50%. The true fraction is most likely between these values.

Supplementary Figure 4. Histograms of the time between viral binding and stage II movement (**a**), the time between stage II movement and viral fusion (**b**), and the distance between the fusion site and the nuclear envelope (**c**) for viruses that enter via clathrin-dependent and -independent endocytosis.

Supplementary Figure 1

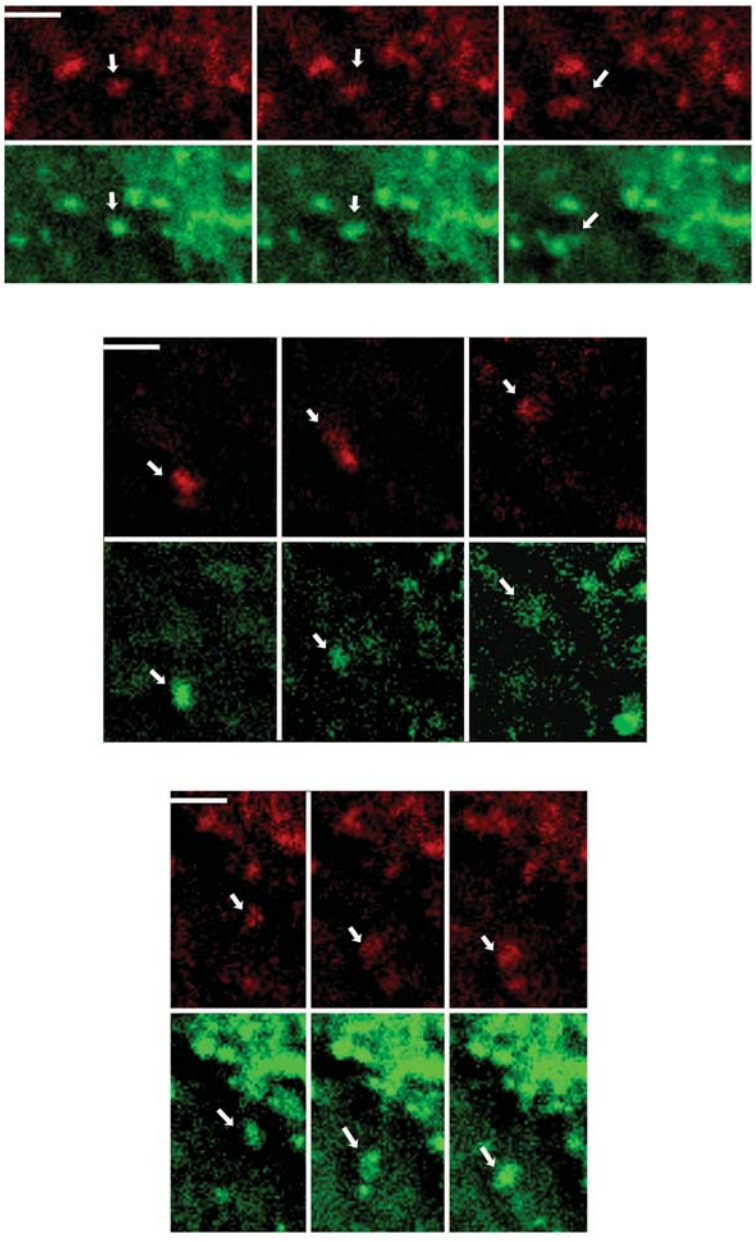

Supplementary Figure 2

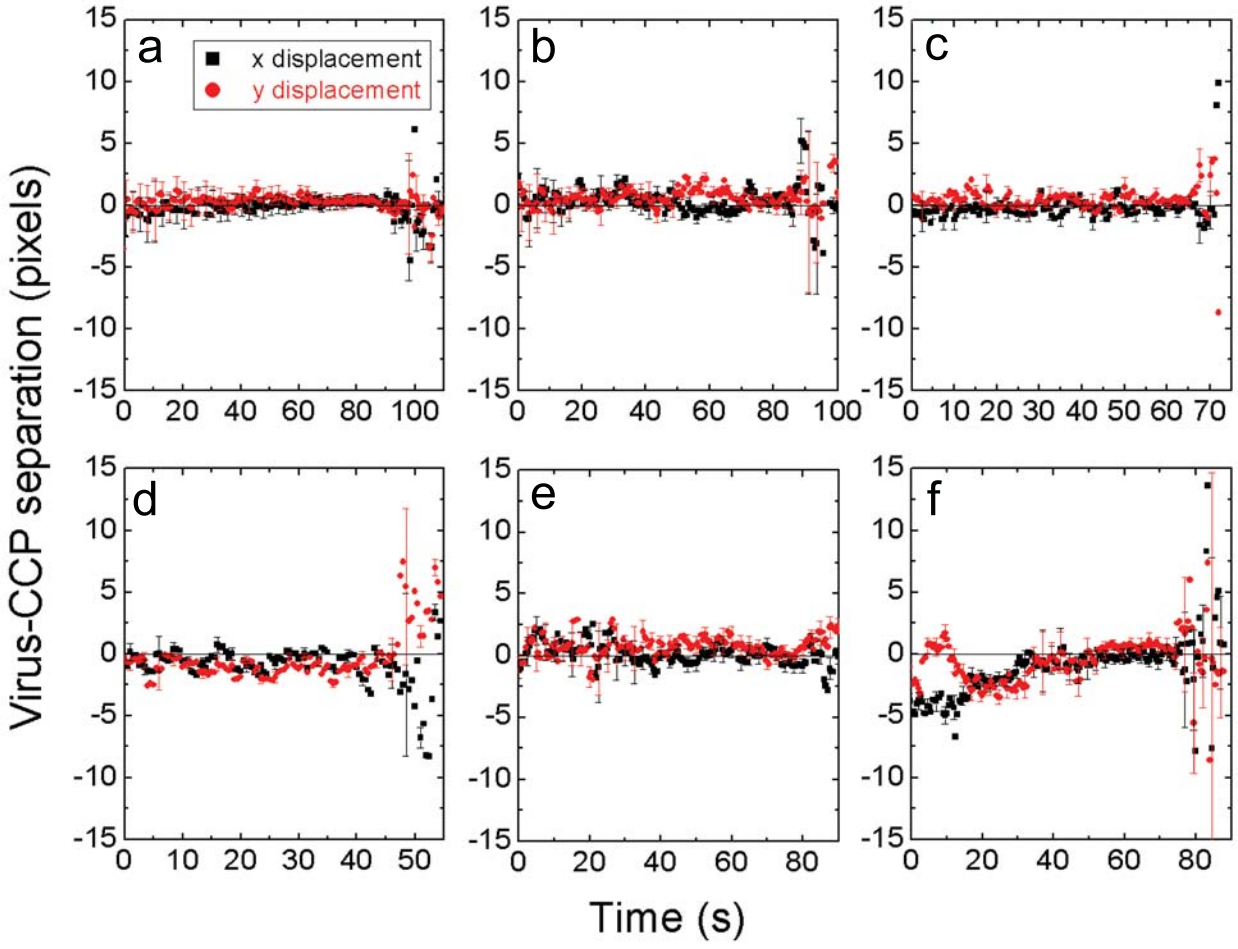

Supplementary Figure 3

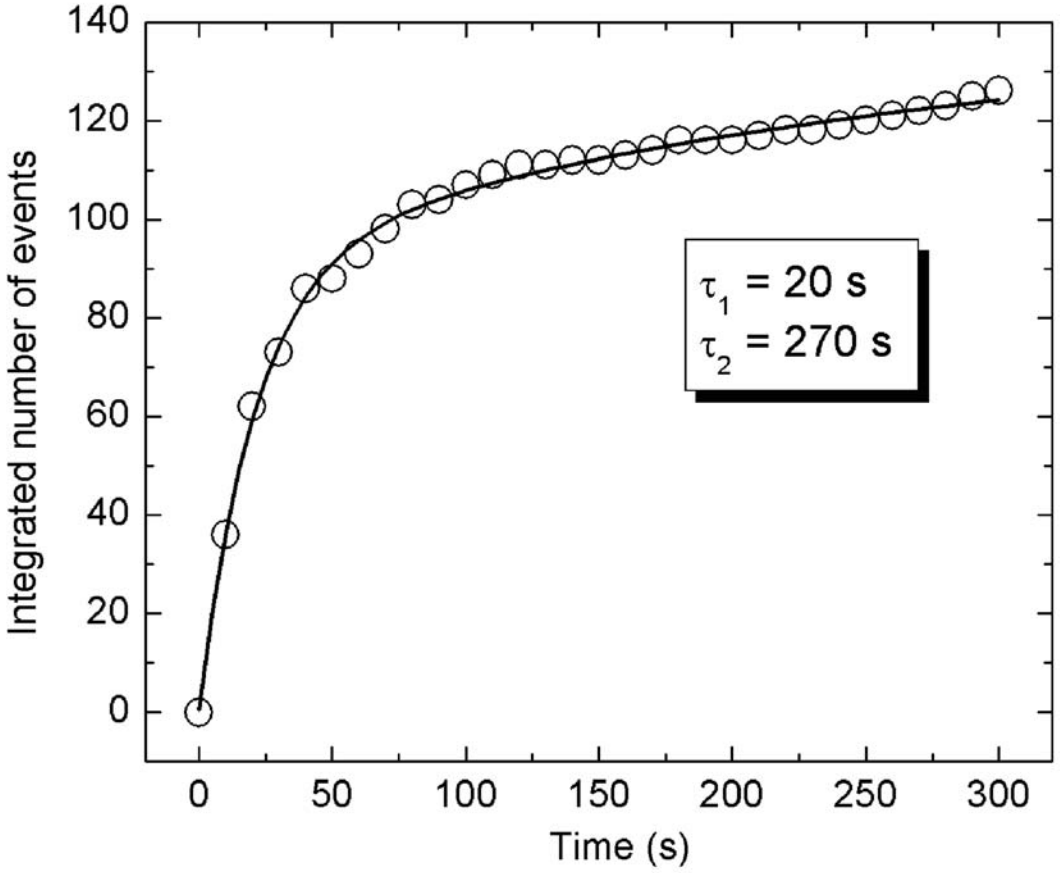

Supplementary Figure 4

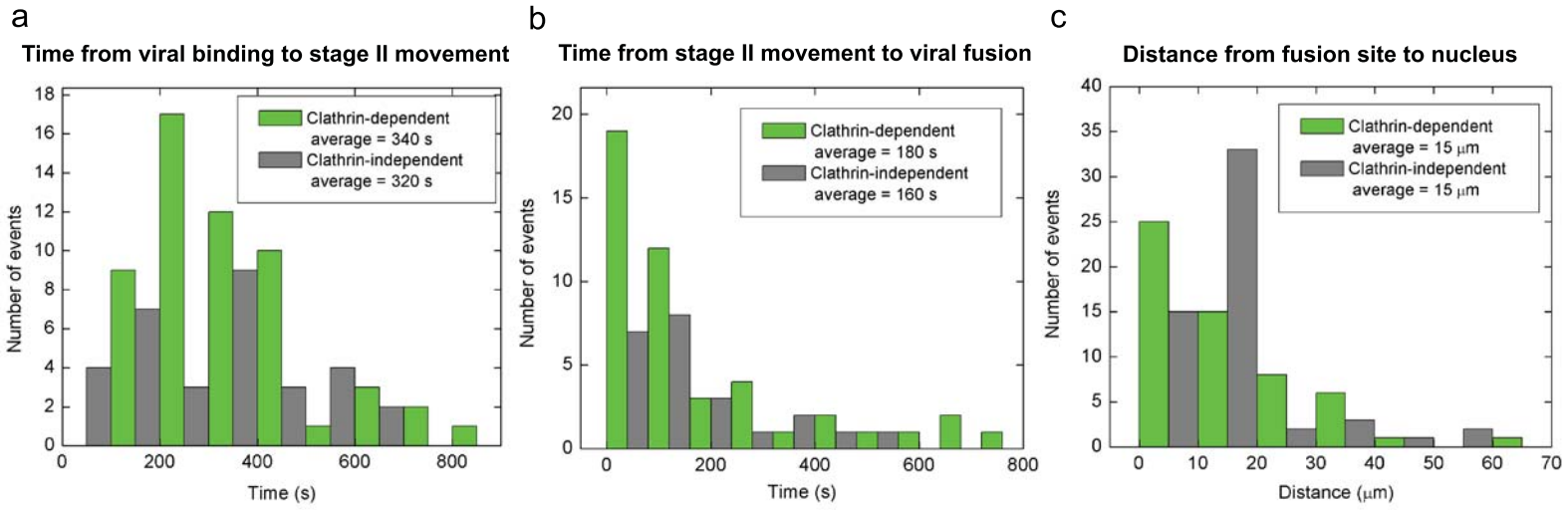

Supplementary Videos:

Videos were taken under the following imaging condition. For **Videos 1–5**, the excitation laser for the EYFP-clathrin or Caveolin-1-EGFP was turned on for 0.5 s every 1.5 s while that for the DiD-labeled viruses was always on. The camera integration time for each frame is 0.5 s. All camera pixels were read out individually. For **Videos 6** and **7**, the excitation laser for the EYFP-clathrin was turned on for 0.5 s every 1.5 s while that for the DiD-viruses was turned on for 0.5 s every 1s. The pixels were binned in a 2x2 fashion. **Videos 6** and **7** thus do not allow an accurate determination of whether CCPs form at or off the virus-binding sites, but are only meant to show that both clathrin-dependent and -independent endocytosis can lead to viral fusion.

All videos are processed by subtracting the low-spatial frequency background signal generated by cytoplasmic EYFP-clathrin or Caveolin-1-EGFP. The videos are compressed significantly and compression compromises video quality.

As the viruses were added to the cells *in situ* the binding of viruses to cells is highly asynchronous. Thus some viruses appear to move only slowly while the circled viruses show the specified behavior of three-stage movement. These slow-moving viruses in the field of view are either in stage I or in stage III during the exhibited time window.

Supplementary Video 1. A dual-color movie of EYFP-tagged clathrin structures (green) and DiD-labeled viruses (red) in a live cell.

Supplementary Video 2. A dual-color movie of EGFP-tagged caveolin structures (green) and DiD-labeled viruses (red) in a live cell.

Supplementary Videos 3 and 4. The internalization of influenza viruses via CCPs. Both movies show the *de novo* formation of a CCP (green) around the virus (red, in white circles), the gradual increase of clathrin intensity, and the rapid disappearance of the clathrin signal immediately before the virus exhibit a rapid, unidirectional movement towards the perinuclear region (stage II movement).

Supplementary Video 5. The internalization of an influenza virus without association with a CCP. The virus (red, in a white circle) did not associate with a CCP before its stage-II movement inside the cell.

Supplementary Video 6. The internalization and fusion of an influenza virus (red, in a white circle) after association with a CCP (green). Fusion is indicated by a dramatic increase of the DiD signal (red).

Supplementary Video 7. The internalization and fusion of an influenza virus (red, in a white circle) without association with a CCP.